IJIRCCE

e-ISSN: 2320-9801 | p-ISSN: 2320-9798

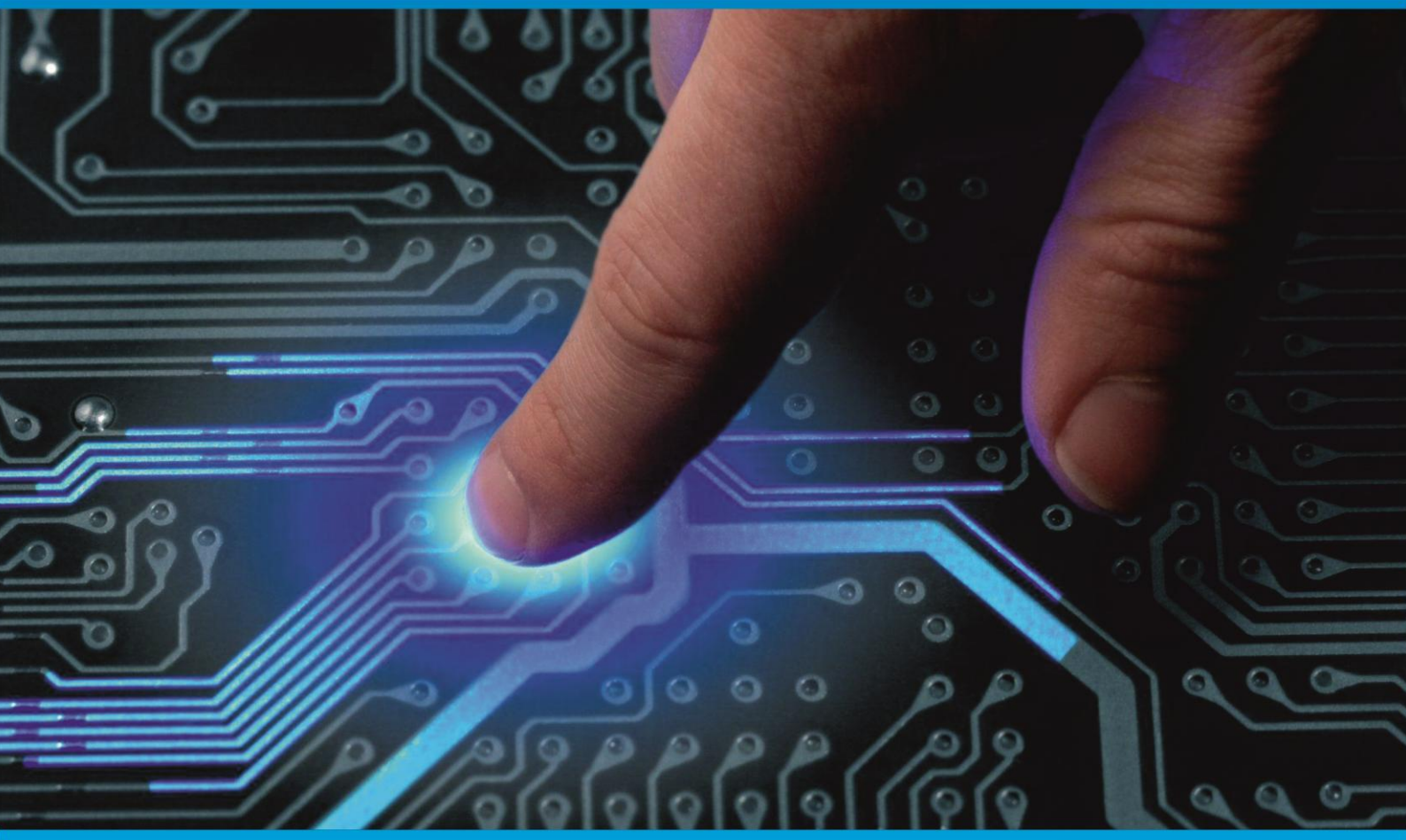

INTERNATIONAL JOURNAL OF INNOVATIVE RESEARCH

IN COMPUTER & COMMUNICATION ENGINEERING

Volume 9, Issue 3, March 2021

INTERNATIONAL STANDARD SERIAL NUMBER INDIA

Impact Factor: 7.488

International Journal of Innovative Research in Computer and Communication Engineering

| e-ISSN: 2320-9801, p-ISSN: 2320-9798| www.ijircce.com | |Impact Factor: 7.488 |

|| Volume 9, Issue 3, March 2021 ||

| DOI: 10.15680/IJIRCCE.2021.0903043|

To Predict the Brightness of Terrain & Cloud Pixels in Remote Sensing Image

M.Dhurgadevi, S.Kavitha.,Msc.,M.Phil

Student, Dept. of Computer Science, Sakthi College of Arts and Science for Women, Oddanchatram, TamilNadu, India

Assistant Professor, Dept. of Computer Science, Sakthi College of Arts and Science for Women, Oddanchatram, TamilNadu, India

ABSTRACT: Next-generation orbital imaging spectrometers will generate unprecedented data volumes, demanding new methods to optimize storage and communication resources. Here, we demonstrate that onboard analysis can excise cloud-contaminated scenes, reducing data volumes while preserving science return. We calculate optimal cloud-screening parameters in advance, exploiting stable radiometric calibration and foreknowledge of illumination and viewing geometry. Channel thresholds expressed in raw instrument values can be then uploaded to the sensor where they execute in real time at gigabit-per-second (Gb/s) data rates. We present a decision theoretic method for setting these instrument parameters and characterize performance using a continuous three-year image archive from the "classic" Airborne Visible/Infrared Imaging Spectrometer (AVIRIS-C). We then sim- ulate the system onboard the International Space Station, where it provides factor-of-two improvements in data volume with negligi- ble false positives. Finally, we describe a real-time demonstration onboard the AVIRIS Next Generation (AVIRIS-NG) flight plat- form during a recent science campaign. In this blind test, cloud screening is performed without error while keeping pace with instrument data rates.

I. INTRODUCTION

The detection of clouds in satellite imagery has a number of important applications in weather and climate studies. The presence of clouds can alter the energy budget of the Earth-atmosphere system through scattering and absorption of shortwave radiation and the absorption and re-emission of infrared radiation. The scattering and absorption characteristics of clouds vary with the microphysical properties of clouds, hence the cloud type. Thus, detecting the presence of clouds over a region in satellite imagery is important in order to derive atmospheric (e.g., optical depth, phase, temperature, etc.) that give insight into weather and climate processes. For many applications however, clouds are a contaminant whose presence interferes with retrieving atmosphere or surface information. In these cases, the detection of cloud contaminated pixels in satellite imagery is important to isolate cloud-free pixels used to retrieve atmospheric thermodynamic information (e.g., temperature and moisture information, ozone content, and even trace gas concentrations) or surface geophysical parameters (e.g., land and sea surface temperature, vegetation information, etc.) from cloudy ones.

The ability to derive an accurate cloud mask from geostationary and polar orbiting satellite data under a variety of conditions has been a research topic since the launch of the first Earth observing satellite TIROS-1 in 1960. The limited success of some early studies (Coakley and Bretherton 1982, Rossow and Garder 1993, and those discussed by Goodman and Sellers 1988) suggests that the accurate detection of clouds in satellite imagery both during the day and at night is a challenging problem. In more recent work, the probability of detecting clouds has been reported to exceed 90% (Saunders and Kriebel 1988, Merchant et al. 2005, Jedlovec et al. 2008, Reuter et al. 2009) but the performance varies seasonally, regionally, with time of day and retrieval technique. While traditionally both spatial and spectral techniques have been employed to identify cloud contaminated pixels in polar orbiting and geostationary satellite data, sensor spatial resolution, the lack of surface – atmospheric boundary layer temperature contrast, and surface emissivity variations all present performance challenges to a given cloud detection approach. Thus, any one technique may not be best suited for all applications, but may perform quite well in a particular environment (usually the environment in which the algorithm was developed and tested). The key to the success of most of these algorithms lies in the selection of the thresholds for various spectral tests. In more robust algorithms, spatially and temporally varying thresholds, which better capture local atmospheric and surface effects, are used to improve their performance and broaden their application over algorithms with fixed thresholds for cloud tests.

In this chapter, a review of several multispectral cloud detection techniques is presented. Emphasis is placed on techniques which use multispectral approaches applicable to a wide variety of current and future satellite sensors.

| e-ISSN: 2320-9801, p-ISSN: 2320-9798| www.ijircce.com | |Impact Factor: 7.488 |

|| Volume 9, Issue 3, March 2021 ||

| DOI: 10.15680/IJIRCCE.2021.0903043|

The detailed methodology used in several recent and widely used algorithms is highlighted. The performance of two cloud detection approaches is compared for the same observational conditions.

II. LITERATURE SURVEY

We focus on the VSWIR electromagnetic spectrum from 0.4–2.5 μm. Fig. 1 shows an example scene from the "classic" Airborne Visible/Infrared Imaging Spectrometer (AVIRIS-C) with representative spectra of different materials and clouds. There are many studies of cloud detection in these wavelengths,

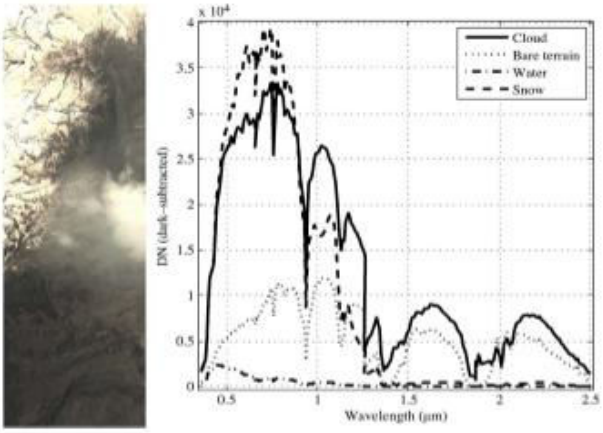

Fig. 1. (Left) AVIRIS-C image f100521t02p05, a challenging scene that contains both clouds and snow. (Right) Spectra from bare terrain, snow, open water, and clouds, in units of dark-subtracted instrument digital numbers (DNs).

and algorithms vary in their assumptions and complexity. "Classical" cloud screening applies threshold tests to spatial and spectral properties of the image. Pixels whose values fall outside valid ranges are marked as cloudy. For example, the MODIS algorithm compares selected visible and near- infrared (VNIR) and near-infrared (NIR) bands to predetermined thresholds and then aggregates the result in different combinations depending on land type. The algorithm uses a combination of 14 wavelengths and over 40 tests. This underscores the intrinsic difficulty of constructing a universal and complete cloud-screening procedure. Even more complex algorithms are possible. Some state- of-the-art cloud-screening techniques estimate the optical path from absorption features such as the oxygen A band, as in Gómez-Chova et al. or Taylor et al. Thermal infrared (IR) channels can add brightness temperature information. Minnis et al. predict clear-sky brightness temperature values using ambient temperature and humidity and then excise pixels outside these intervals. Texture cues can be also used to recognize clouds by their high spatial heterogeneity. Martins et al. demonstrate that a simple spatial analysis, i.e., the standard deviation of VNIR isotropic reflectances in a 3×3 pixel window, reliably discriminates clouds from aerosol plumes over ocean scenes.

B. Algorithm Requirements

Previous systems try to screen all clouds to prevent con- tamination of later retrieval algorithms. In contrast, we aim to reduce the instrument data volume, which leads to distinct requirements. Completeness is not critical since the end user can perform more precise cloud screening later. Our algorithm can be conservative, abstaining from ambiguous classifications to prevent loss of science data. This requires some way to represent classification certainty. The Bayesian probabilistic model of Merchant et al. combines observational data with prior predictions from atmospheric forecasts, leading to true probabilistic predictions. Onboard cloud screening must also satisfy strict computa- tional constraints. The algorithm must process all data collected by the spectrometer before it enters the flight recorder. In many cases, this requires that the algorithm run in instrument hardware such as a field-programmable gate array (FPGA), entailing additional design requirements.

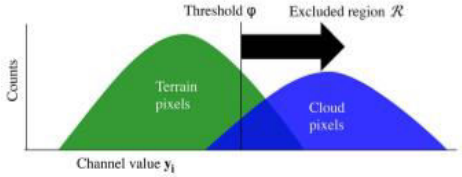

Fig. 2. Thresholds φ define an exclusion region to classify pixels as cloudy thresholds.

| e-ISSN: 2320-9801, p-ISSN: 2320-9798| www.ijircce.com | |Impact Factor: 7.488 |

|| Volume 9, Issue 3, March 2021 ||

| DOI: 10.15680/IJIRCCE.2021.0903043|

A cloud-screening testbed was installed in parallel with the regular AVIRIS-NG data system and operated without error during a recent science campaign.

III. SYSTEM ANALYSIS

3.1 PROBLEM IDENTIFICATION

As mentioned in Section pixel-level data necessarily has fewer dimensions than multi-pixel windows, which can make reliable detection of cloud more difficult. This is exacerbated in RGB when compared to multispectral data, because high albedo terrains (bright urban areas, for example) look the same in RGB as cloud pixels do, when they are be more separable in NIR and TIR bands. Although individual pixels can be misleading over certain terrains, texture often varies greatly between cloud and non-cloud. Therefore, if the system is to perform robustly in high albedo terrains, we need to extract spatial features around each pixel, as well as the individual pixel values themselves, and combine their information content to help distinguish cloud and non-cloud by their texture and surrounding context. Fusion of these different features is vital, because using only high-level features may make it difficult to learn simpler relationships based on colour and brightness. Using an FCN with residual connections in the style of U-net achieves these aims, whilst allowing the entire model to be optimised end-to-end during the training phase.

3.2 EXISTING SYSTEM

In Existing input, CloudFCN(Fully Convolutional Network) takes extended scenes from satellite imagery with arbitrary spatial dimensions. For each given spectral band combination (e.g., RGB) a different instance of the model is needed, however the only alteration made to the design is the number of input channels—no internal parameters are altered. The output of the model has the same spatial size as the input, but can take two distinct formats. When a pixel-by-pixel mask is desired, the final layer uses a softmax activation to classify each pixel as Clear or Cloudy. This is advantageous because it can be easily extended to multi-class problems (e.g., Clear vs. Cloud vs. Cloud Shadow). However, when cloud coverage estimation (as in the percentage of cloud cover over a whole scene) is the desired final product, we output a mask where each pixel has a value between 0 (clear) and 1 (thick cloud), and the cloudiness of a pixel is treated as a regression problem. We then take an average over the whole scene for the cloud coverage estimation. This format allows the model to make estimates for thin cloud as well as thick, and results in more accurate percentages through averaging.

3.3 PROPOSED SYSTEM

The proposed model has several desirable traits, which alleviate the issues that other methods exhibit. First, our design allows for flexible input formats, having no specific spectral requirements, and is able to ingest input images of different sizes. Second, we combine the simplest brightness and colour information with more abstract and complex features from the surrounding areas, creating a complementary set of features that exhibit the strengths of both pixel-level techniques and convolutional ones. Lastly, the output format of the model, and attendant loss function, can be selected based on user needs, increasing the number of possible applications for the method, from cloud coverage estimation (in which a RMSE loss is used) to pixel-wise masking (with a categorical-crossentropy loss).

IV. SYSTEM IMPLEMENTATION

4.1 Lossy Algorithms:

As with lossless algorithms, lossy algorithms also look for repeat pixel values and assign less data to common values. If we take a photo of a sunset over the sea, for example there are going to be groups of pixels with the same colour value, which can be reduced. Lossy algorithms tend to be more complex, as a result they achieve better results for bitmaps and can accommodate for the lose of data. The compressed file is an estimation of the original data. Other advantages of lossy compression is that it can reduce file sizes much more than lossless compression and you can determine how much compression can be applied. For example JPEG is a lossy format and GIF is lossless. With JPEG you can determine how much compression is applied, whereas with GIF you can't, it's set for you. Also JPEG can compress files much more than GIFs - JPEGs can reduce a file to up to 5% of its original size. One of the disadvantages of lossy compression is that if the compressed file keeps being compressed, then the quality will degraded drastically. The diagram alongside illustrates this process.

MERIS/AATSR cloud-screening algorithm is being implemented as an independent module AATSR(Advanced Along Track Scanning Radiometer) and MERIS (Medium Resolution Imaging Spectrometer)

| e-ISSN: 2320-9801, p-ISSN: 2320-9798| www.ijircce.com | |Impact Factor: 7.488 |

|| Volume 9, Issue 3, March 2021 ||

| DOI: 10.15680/IJIRCCE.2021.0903043|

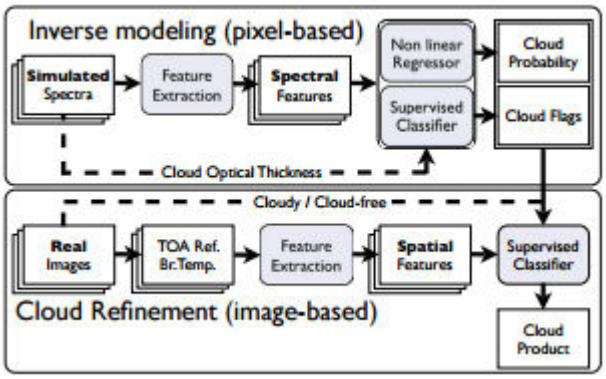

The proposed cloud-screening scheme relies on the extraction of meaningful physical features (e.g. brightness, whiteness, temperature) that are combined with atmospheric absorption features at specific spectral band locations (oxygen and water vapour absorptions). The cloud-screening algorithm should be capable of detecting clouds accurately, but also and very importantly, it provides a cloud probability or cloud contamination index per pixel rather than binary flags. This added value product allows the user to obtain an adjustable cloud mask depending on the further processing stages and final use of the image.

4.2 Color Feature Extraction

Color feature is extracted by Color Histogram and Color Descriptor. The Color histogram specifies the colorpixel distribution in an image. Color histogram uses two types of color space that are RGB, HSV. ColorHistogram (CH), contains occurrences of each color obtained by counting all image pixels having that color. Each pixel is associated to a specific histogram bin only on the basis of its own color, and color similarity across different bins or color dissimilarity in the same bin is not taken into account. Since any pixel in the image can be described by three components in a certain color space (for instance, red, green and blue components in RGB space or hue, saturation and value in HSV space), a histogram, i.e., the distribution of the number of pixels for each quantized bin, can be defined for each component. Color descriptor consists the color expectancy, color variance and color skewness. Color expectancy is the average or mean of intensity in image. Color variance is the square root of the standard deviation. Color skewness is a measure of the asymmetry of the probability distribution of a real valued random variable. Two types of skewness are Positive skewness and Negative skewness.

4.3 Texture Feature Extraction

An image texture is a set of metrics calculated in image processing designed to quantify the perceived textureof an image. Image Texture gives us information about the spatial arrangement of color or intensities in an image or selected region of an image. Texture analysis attempts to quantify intuitive qualities described by terms such as rough, smooth, silky, or bumpy as a function of the spatial variation in pixel intensities. In this sense, thoroughness or bumpiness refers to variations in the intensity values, or gray levels.

4.4 Comparison with Other Target Detection Methods

In order to evaluate the results of the proposed detection approach, three common target detection techniques, including ACE, CEM, and MF, were implemented on the Meteosat multispectral images. The color composite of the visible and near infrared spectral bands (VIS: 0.8, VIS: 0.6, IR: 8.7 μm) is shown in Figure 2.

After introducing the multispectral image in Figure 2 and selecting the ROIs manually (from two specific cloud and no-cloud targets), the three above-mentioned detection algorithms were implemented. For this purpose, the average cloud spectrum based on the selected ROIs in cloudy regions was first produced. The mean cloud signal obtained from the selected cloudy ROIs is shown in Figure 13. This spectrum is used as training spectra, which will be used as input in the detection models. By the way, it should be mentioned that a minimum noise fraction (MNF) transform was also implemented on the raw multispectral image to reduce the spectral noise. Afterwards, the set of detection algorithms were performed respectively on the images. Figure 14 represents the resulting detection outputs from these algorithms in a smaller subset of our study area.

| e-ISSN: 2320-9801, p-ISSN: 2320-9798| www.ijircce.com | |Impact Factor: 7.488 |

|| Volume 9, Issue 3, March 2021 ||

| DOI: 10.15680/IJIRCCE.2021.0903043|

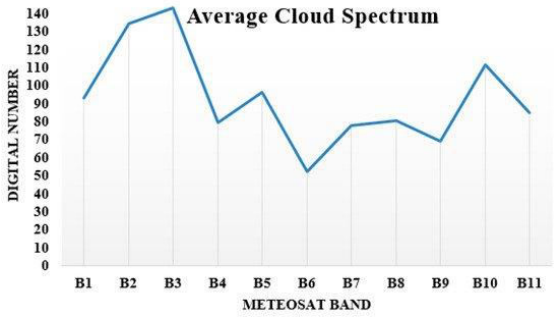

Figure 13. Averaged cloud spectrum obtained from the mean value of the cloud Regions Of Interest (ROI) visually selected on the Meteosat image of the same area.

V. CONCLUSION

This paper has described a novel method for cloud screening onboard spacecraft at Gb/s data rates. We perform the most challenging computations on the ground, exploiting foreknowl- edge of observation geometry and surface type to predict the brightness of terrain pixels and cloud pixels. We calculate optimal thresholds in uncalibrated instrument values that can be uploaded for real-time execution by the flight system.. One could always design a more complex cloud classifier to disambiguate the most difficult pixels and consequently achieve a slight improvement in data volume reduction. However, our simple algorithm already achieves better than 90% of the theoretical maximum making it sufficient for many applica- tions and a useful point on the design trade space. At a time when communications and storage subsystems struggle under increasing data rates, the potential for onboard cloud screening has remained relatively unstudied. Mission designers should bear in mind that a few simple design considerations, i.e., the introduction of channel and aggregation thresholds, can enable factor-of-two reductions in data volume.

VI. FUTURE ENHANCEMENT

Future work could seek alternative representations that scale better with dimensionality. A more promising approach would be to incorporate additional domain knowledge into the state vector. One could condition thresholds on very specific land types or on real-time cloud products like the GOES cloud mask. Preprocessing and feature extraction could also improve performance. For example, one could compute spectral derivatives; sums, differences, or ratios of channels; or continuum-relative absorption band depths [47]. Such spectral features could potentially improve results at a low computational cost.

REFERENCES

1. King, M.D.; Platnick, S.; Menzel, W.P.; Ackerman, S.A.; Hubanks, P. Spatial and Temporal Distribution of Clouds Observed by MODIS Onboard the Terra and Aqua Satellites. *IEEE Trans. Geosci. Remote Sens.* 2013, *51*, 3826–3852. [Google Scholar] [CrossRef]
2. Xue, J.; Su, B. Significant remote sensing vegetation indices: A review of developments and applications. *J. Sens.* 2017, *2017*, 1353691. [Google Scholar] [CrossRef]
3. Larsen, S.; Koren, H.; Solberg, R. Traffic Monitoring using Very High Resolution Satellite Imagery. *Photogramm. Eng. Remote Sens.* 2009, *75*, 859–869. [Google Scholar] [CrossRef]
4. Di Girolamo, L.; Davies, R. Cloud fraction errors caused by finite resolution measurements. *J. Geophys. Res. Atmos.* 1997, *102*, 1739–1756. [Google Scholar] [CrossRef]
5. Ronneberger, O.; Fischer, P.; Brox, T. U-Net: Convolutional Networks for Biomedical Image Segmentation. In *Medical Image Computing and Computer-Assisted Intervention*; Springer: Cham, Switzerland, 2015. [Google Scholar]
6. Zhang, Z.; Liu, Q.; Wang, Y. Road extraction by deep residual u-net. *IEEE Geosci. Remote Sens. Lett.* 2018, *15*, 749–753. [Google Scholar] [CrossRef]
7. Dong, H.; Yang, G.; Liu, F.; Mo, Y.; Guo, Y. Automatic brain tumor detection and segmentation using U-Net based fully convolutional networks. In *Annual Conference on Medical Image Understanding and Analysis*; Springer: Cham, Switzerland, 2017; pp. 506–517. [Google Scholar]

| e-ISSN: 2320-9801, p-ISSN: 2320-9798| www.ijircce.com | |Impact Factor: 7.488 |

|| Volume 9, Issue 3, March 2021 ||

| DOI: 10.15680/IJIRCCE.2021.0903043|

8. Szegedy, C.; Liu, W.; Jia, Y.; Sermanet, P.; Reed, S.; Anguelov, D.; Erhan, D.; Vanhoucke, V.; Rabinovich, A. Going deeper with convolutions. In Proceedings of the IEEE Computer Society Conference on Computer Vision and Pattern Recognition, Boston, MA, USA, 7–12 June 2015; pp. 1–9. [Google Scholar] [CrossRef]
9. Francis, A.M.; Sidiropoulos, P.; Vazquez, E.; Space, M. Real-Time Cloud Detection in High-Resolution Videos: Challenges and Solutions. In Proceedings of the 6th International Workshop on On-Board Payload Data Compression, Matera, Italy, 20–21 September 2018. [Google Scholar]
10. Jin, S.; Homer, C.; Yang, L.; Xian, G.; Fry, J.; Danielson, P.; Townsend, P.A. Automated cloud and shadow detection and filling using two-date Landsat imagery in the USA. *Int. J. Remote Sens.* 2013, *34*, 1540–1560. [Google Scholar] [CrossRef]
11. Ancuti, C.O.; Ancuti, C.; Hermans, C.; Bekaert, P. A fast semi-inverse approach to detect and remove the haze from a single image. In *Asian Conference on Computer Vision*; Springer: Berlin/Heidelberg, Germany, 2010; pp. 501–514. [Google Scholar]
12. Makarau, A.; Richter, R.; Müller, R.; Reinartz, P. Haze detection and removal in remotely sensed multispectral imagery. *IEEE Trans. Geosci. Remote Sens.* 2014, *52*, 5895–5905. [Google Scholar] [CrossRef]
13. Gultepe, I.; Zhou, B.; Milbrandt, J.; Bott, A.; Li, Y.; Heymsfield, A.J.; Ferrier, B.; Ware, R.; Pavolonis, M.; Kuhn, T.; et al. A review on ice fog measurements and modeling. *Atmos. Res.* 2015, *151*, 2–19. [Google Scholar] [CrossRef]
14. Zhang, Q.; Xiao, C. Cloud detection of RGB color aerial photographs by progressive refinement scheme. *IEEE Trans. Geosci. Remote Sens.* 2014, *52*, 7264–7275. [Google Scholar] [CrossRef]
15. Fisher, A. Cloud and cloud-shadow detection in SPOT5 HRG imagery with automated morphological feature extraction. *Remote Sens.* 2014, *6*, 776–800. [Google Scholar] [CrossRef]
16. Pahlevan, N.; Roger, J.C.; Ahmad, Z. Revisiting short-wave-infrared (SWIR) bands for atmospheric correction in coastal waters. *Opt. Express* 2017, *25*, 6015–6035. [Google Scholar] [CrossRef] [PubMed]
17. Chylek, P.; Robinson, S.; Dubey, M.; King, M.; Fu, Q.; Clodius, W. Comparison of near-infrared and thermal infrared cloud phase detections. *J. Geophys. Res. Atmos.* 2006, *111*. [Google Scholar] [CrossRef]
18. Gultepe, I.; Sharman, R.; Williams, P.D.; Zhou, B.; Ellrod, G.; Minnis, P.; Trier, S.; Griffin, S.; Yum, S.S.; Gharabaghi, B.; et al. A review of high impact weather for aviation meteorology. *Pure Appl. Geophys.* 2019, *176*, 1869–1921. [Google Scholar] [CrossRef]
19. Irish, R.R.; Barker, J.L.; Goward, S.N.; Arvidson, T. Characterization of the Landsat-7 ETM+ Automated Cloud-Cover Assessment (ACCA) algorithm. *Photogramm. Eng. Remote Sens.* 2006, *72*, 1179–1188. [Google Scholar] [CrossRef]

INNO SPACE

SJIF Scientific Journal Impact Factor

Impact Factor:
7.488

ISSN INTERNATIONAL STANDARD SERIAL NUMBER INDIA

निस्केयर NISCAIR

INTERNATIONAL JOURNAL OF INNOVATIVE RESEARCH

IN COMPUTER & COMMUNICATION ENGINEERING

9940 572 462 6381 907 438 ijircce@gmail.com

www.ijircce.com

Scan to save the contact details